Specimen alignment with limited point-based homology: 3D morphometrics of disparate bivalve shells (Mollusca: Bivalvia) (#71498)

First submission

Guidance from your Editor

Please submit by **30 Mar 2022** for the benefit of the authors (and your $200 publishing discount) .

Structure and Criteria
Please read the 'Structure and Criteria' page for general guidance.

Author notes
Have you read the author notes on the guidance page?

Raw data check
Review the raw data.

Image check
Check that figures and images have not been inappropriately manipulated.

Privacy reminder: If uploading an annotated PDF, remove identifiable information to remain anonymous.

Files

Download and review all files from the materials page.

7 Figure file(s)
1 Table file(s)
1 Other file(s)

Structure and Criteria

2

Structure your review

The review form is divided into 5 sections. Please consider these when composing your review:

1. **BASIC REPORTING**
2. **EXPERIMENTAL DESIGN**
3. **VALIDITY OF THE FINDINGS**
4. General comments
5. Confidential notes to the editor

You can also annotate this PDF and upload it as part of your review

When ready [submit online](#).

Editorial Criteria

Use these criteria points to structure your review. The full detailed editorial criteria is on your [guidance page](#).

BASIC REPORTING

Clear, unambiguous, professional English language used throughout.

Intro & background to show context. Literature well referenced & relevant.

Structure conforms to [PeerJ standards](#), discipline norm, or improved for clarity.

Figures are relevant, high quality, well labelled & described.

Raw data supplied (see [PeerJ policy](#)).

EXPERIMENTAL DESIGN

Original primary research within [Scope of the journal](#).

Research question well defined, relevant & meaningful. It is stated how the research fills an identified knowledge gap.

Rigorous investigation performed to a high technical & ethical standard.

Methods described with sufficient detail & information to replicate.

VALIDITY OF THE FINDINGS

Impact and novelty not assessed. *Meaningful* replication encouraged where rationale & benefit to literature is clearly stated.

All underlying data have been provided; they are robust, statistically sound, & controlled.

Conclusions are well stated, linked to original research question & limited to supporting results.

Standout reviewing tips

The best reviewers use these techniques

Tip	Example
Support criticisms with evidence from the text or from other sources	*Smith et al (J of Methodology, 2005, V3, pp 123) have shown that the analysis you use in Lines 241-250 is not the most appropriate for this situation. Please explain why you used this method.*
Give specific suggestions on how to improve the manuscript	*Your introduction needs more detail. I suggest that you improve the description at lines 57- 86 to provide more justification for your study (specifically, you should expand upon the knowledge gap being filled).*
Comment on language and grammar issues	*The English language should be improved to ensure that an international audience can clearly understand your text. Some examples where the language could be improved include lines 23, 77, 121, 128 – the current phrasing makes comprehension difficult. I suggest you have a colleague who is proficient in English and familiar with the subject matter review your manuscript, or contact a professional editing service.*
Organize by importance of the issues, and number your points	*1. Your most important issue* *2. The next most important item* *3. ...* *4. The least important points*
Please provide constructive criticism, and avoid personal opinions	*I thank you for providing the raw data, however your supplemental files need more descriptive metadata identifiers to be useful to future readers. Although your results are compelling, the data analysis should be improved in the following ways: AA, BB, CC*
Comment on strengths (as well as weaknesses) of the manuscript	*I commend the authors for their extensive data set, compiled over many years of detailed fieldwork. In addition, the manuscript is clearly written in professional, unambiguous language. If there is a weakness, it is in the statistical analysis (as I have noted above) which should be improved upon before Acceptance.*

Specimen alignment with limited point-based homology: 3D morphometrics of disparate bivalve shells (Mollusca: Bivalvia)

Stewart M Edie [Corresp., 1] , **Katie S Collins** [2] , **David Jablonski** [3, 4]

[1] Department of Paleobiology, National Museum of Natural History, Smithsonian Institution, Washington, DC, United States

[2] Department of Earth Sciences, Invertebrates and Plants Palaeobiology Division, Natural History Museum, London, United Kingdom

[3] Department of the Geophysical Sciences, University of Chicago, Chicago, IL, United States

[4] Committee on Evolutionary Biology, University of Chicago, Chicago, IL, United States

Corresponding Author: Stewart M Edie
Email address: edies@si.edu

Comparative morphology fundamentally relies on the orientation and alignment of specimens. In the era of geometric morphometrics, point-based homologies are commonly deployed to register specimens and their landmarks in a shared coordinate system. However, the number of point-based homologies commonly diminishes with increasing phylogenetic breadth. These situations invite alternative, often conflicting, approaches to alignment. The bivalve shell (Mollusca: Bivalvia) exemplifies a homologous structure with few universally homologous points—only one can be identified across the Class, the shell 'beak.' Here, we develop an axis-based framework, grounded in the homology of shell features, to orient shells for landmark-based, comparative morphology. As the choice of homologous points for alignment can affect shape differences among specimens, so can the choice of orientation axes. Analysis of forty-five possible alignment schemes finds general conformity among the shape differences of 'typical' equilateral shells, but the shape differences among atypical shells can change considerably, particularly those with distinctive modes of growth. Each alignment implies a hypothesis about the ecological, developmental, or evolutionary basis of morphological differences, but we recognize one alignment in particular as a continuation of the historical approaches to morphometrics of shell form: orientation via the hinge line. Beyond bivalves, this axis-based approach to aligning specimens facilitates the comparison of continuous differences in shape among many other phylogenetically broad and morphologically disparate samples.

1 **TITLE:** Specimen alignment with limited point-based homology: 3D morphometrics of
2 disparate bivalve shells (Mollusca: Bivalvia)

3 **RUNNING HEAD:** Aligning bivalve shells

4 **KEYWORDS:** marine bivalve, shell shape, geometric morphometrics, 3D morphometrics,
5 anatomical homology

6 **AUTHORS:** Stewart M. Edie[1]*, Katie S. Collins[2], David Jablonski[3,4]

7 [1] Department of Paleobiology, National Museum of Natural History, Smithsonian Institution,
8 Washington, DC, 20013, U.S.A.

9 [2] Natural History Museum, London, London, SW7 5BD, United Kingdom

10 [3] Department of the Geophysical Sciences, University of Chicago, 5734 South Ellis Ave,
11 Chicago, IL 60637, USA.

12 [4] Committee on Evolutionary Biology, University of Chicago, Chicago, IL 60637, USA

13 * corresponding author

1. Abstract

15 Comparative morphology fundamentally relies on the orientation and alignment of specimens. In
16 the era of geometric morphometrics, point-based homologies are commonly deployed to register
17 specimens and their landmarks in a shared coordinate system. However, the number of point-
18 based homologies commonly diminishes with increasing phylogenetic breadth. These situations
19 invite alternative, often conflicting, approaches to alignment. The bivalve shell (Mollusca:
20 Bivalvia) exemplifies a homologous structure with few universally homologous points—only
21 one can be identified across the Class, the shell 'beak.' Here, we develop an axis-based
22 framework, grounded in the homology of shell features, to orient shells for landmark-based,
23 comparative morphology. As the choice of homologous points for alignment can affect shape
24 differences among specimens, so can the choice of orientation axes. Analysis of forty-five
25 possible alignment schemes finds general conformity among the shape differences of 'typical'
26 equilateral shells, but the shape differences among atypical shells can change considerably,
27 particularly those with distinctive modes of growth. Each alignment implies a hypothesis about
28 the ecological, developmental, or evolutionary basis of morphological differences, but we
29 recognize one alignment in particular as a continuation of the historical approaches to
30 morphometrics of shell form: orientation via the hinge line. Beyond bivalves, this axis-based
31 approach to aligning specimens facilitates the comparison of continuous differences in shape
32 among many other phylogenetically broad and morphologically disparate samples.

2.   Introduction

Comparative morphology depends on how organisms are oriented, or aligned. For a simplistic example, a kiwi's beak is relatively long for a bird when measured from the tip to the base of the skull, but rather short when measured from the tip to the nostrils (an alternative definition of beak length; Borras et al. 2000). Thus, the choice of anatomical reference points can profoundly alter our interpretations of evolutionary morphology. Alignments commonly use point-based aspects of homologous features—the junction of the kiwi's beak with the cranium (a Type I landmark; Bookstein 19   ) and the distal-most point of the beak, the tip (a Type III landmark).
Closely related organisms tend to have more of these homologous points, allowing for a straightforward alignment and comparison of their shapes. Alignment on strict, point-based homology becomes more problematic with increasing phylogenetic distance, however, as the number of homologous features invariably diminishes (Bardua et al. 2019).

Bivalve mollusks have become a model system for macroevolution and macroecology (Jablonski et al. 2017; Edie et al. 2018; Crame 2020), but their strikingly disparate body plans complicate Class-wide morphologic comparisons using strict homology (Cox et al. 1969). Inimical to triangulation and thus alignment via landmarks, the valve of the bivalve shell—the most widely available feature of the animal today and through the fossil record—has only one homologous *point*: the apex of the beak, which is the origin of growth of the embryonic shell at the apex of the beak   arter et al. 2012:21; Figure 1). Homology-free approaches can be useful for comparing the shapes of shell valves when anatomical orientation is either unknown or uncertain (Bailey 2009); but wholesale substitution of shape, i.e. analogy, for homology complicates the evolutionary interpretation of morphological differences. Despite the lack of multiple homologous *points* on the shell valve across the Class, a number of its *features* are homologous and can facilitate comparisons. Here, we apply principles of bivalve comparative morphology to develop a framework for aligning shell valves (hereafter 'shells') across the Class, thus enabling phylogenetically extensive analyses of their shapes using geometric morphometrics despite the remarkable range of body plans across the clade.

2.1   Approaches to orienting the bivalve shell

Many body directions, axes, lines, and planes have been defined for bivalves (see Cox et al. 1969; Bailey 2009; Carter et al. 2012)—some related to features of the shell (an accretionary exoskeleton composed of calcium carbonate; Marin et al. 2012), and others to features of the soft body (the digestive tract, foot, byssus, muscles, etc.). Separation into these 'shell' and 'body' terms is a false   asek 1963*a*) but convenient dichotomy (Yonge 1954): the shell is generated by, and remains attached to, the soft body, but their morphologies can become decoupled (Yonge 1954; Edie et al. 2022). Still, both shell and body features are required for orientation via homology (Stasek 1963*a*; cf. Bailey 2009). Given our goal of aligning the shell for geometric

69   morphometrics across broad phylogenetic scales and through the fossil record, we focus on

70   orientations that can be inferred from this part alone, but we must use a critical body axis to fully

71   determine orientation, the anteroposterior axis. Thus, shell features used for alignment can be

72   divided into two classes: (1) intrinsic characteristics of the shell relating to its geometry, growth,

73   and biomechanics, and (2) proxies of the body recording the positions of the soft anatomy

74   including the adductor muscle scars, pallial line, byssal notch, pedal gape, siphon canal, and

75   more.

2.1.1   Orientation via intrinsic characteristics of the shell

77   Although the only homologous point on the shell across all bivalves is the apex of the beak

78   (hereafter 'beak', Figure 1), aspects of the shell's biomechanics, such as its hinge axis, and its

79   accretionary growth permit orientation via homology. The planes and lines proposed to describe

80   shell geometry and growth have been criticized for their lack of homology (Stasek 1963b:226)

81   and ubiquity across the class (Lison 1949:62; Owen 1952:149; Carter 1967:272). We discuss two

82   such features here, the directive plane and demarcation line (Figure 1 and defined below), but we

83   also address and test two alternative means of orienting shells that combine the shell's geometry

84   and growth: the maximum growth axis and the shape of the shell commissure.

85   Related to the shell's biomechanics, the hinge has been treated as a "fixed dorsal region"

86   (Yonge 1954:448; see also Jackson 1890:282), later redefined to reflect the position of the

87   mantle isthmus bridging between the two valves as a universally dorsal-directed feature (Cox et

88   al. 1969:79). Beyond its determination of dorsoventral directionality, the hinge, specifically the

89   hinge axis defined as the "ideal line drawn through the hinge area, and coinciding with the axis

90   of motion of the valves" (Jackson 1890:309), is a Class-wide feature that can constrain one of the

91   three Cartesian axes required for alignment. In a strictly mechanical sense, the ligament, and not

92   the hinge teeth, directs the orientation of the axis of motion (Trueman 1964:56; Cox et al.

93   1969:47; Stanley 1970:47). However, the hinge area, which includes the teeth, is hypothesized to

94   be analogous in function (Cox et al. 1969:47)—guiding the two valves into alignment during

95   closure—and homologous in its origin (Scarlato and Starobogatov 1978; Waller 1998; Fang and

96   Sanchez 2012). Thus, our definition of the **hinge line** indicates the longest dimension of the

97   hinge area (see 'hinge' in Carter et al. 2012:74 and Figure 1); for quantitatively aligning shells,

98   the hinge line is determined by the two farthest apart articulating elements of the hinge area,

99   excluding lateral teeth, which are variably present among heterodont species (e.g. Mikkelsen et

100 al. 2006:493; Taylor and Glover 2021); definition proposed here is a synthesis of the discussions

101 in Cox et al. 1969:81 and Bradshaw and Bradshaw 1971). Thus, by directing the orientation of

102 the horizontal plane which divides the body into dorsal (towards the beak) and ventral (towards

103 the free edge of the shell) territories, the hinge line can also proxy the anteroposterior axis

104 (Figure 1, Cox et al. 1969:81 and discussion below).

105   Related to the geometry and growth of the shell, the **directive plane** (Lison 1949) was
106   proposed as the only plane passing through the shell that contains the logarithmic planispiral line
107   connecting the beak to a point on the ventral margin (Figure 1); all other radial lines would be
108   logarithmic turbinate spirals (or 'helicospirals'; Stasek 1963b:217). In other words, on a radially
109   ribbed shell, there may be a single rib that lies entirely on a plane when viewed from its origin at
110   the umbo to its terminus on the ventral margin; that plane is orthogonal to the commissural plane
111   for planispiral shells (e.g. many Pectinidae, Figure 1), but lies at increasingly acute angles to the
112   commissural plane with increasing tangential components of growth (i.e. geometric torsion; see
113   the trace of the directive plane on *Chione* in Figure 1 and examples in Cox et al. 1969:86-Figs.
114   70-71). In theory, the directive plane could be used to orient the dorsoventral axis of the shell,
115   but in practice, the feature is not universal across shell morphologies (e.g. the strongly coiled
116   *Glossus humanus* [as *Isocardia cor*] in Lison 1949:62; Owen 1952:149). Cox et al. (1969:87)
117   also remark that the plane cannot "be demonstrated easily by visual inspection if the shell lacks
118   radial ribbing, except in rare specimens with an umbonal ridge that proves to lie within the
119   directive plane." Difficulty in application is no excuse to avoid an approach, but the non-
120   universality of this feature renders it inapplicable to Class-wide comparisons of shell shape.

121   Owen (1952) proposed an alternative to the directive plane: the **demarcation line**
122   (Figure 1; originally termed the 'normal axis' but re-named by Yonge 1955:404). As with the
123   directive plane, the demarcation line serves to orient the dorsoventral direction and separate the
124   shell into anterior and posterior 'territories' (Yonge 1955:404; Morton and Yonge 1964:40), but
125   its definition has been variably characterized in geometric and/or anatomical terms. Per Owen
126   (1952:148), the demarcation line can "be considered with reference to three points: the umbo, the
127   normal zone of the mantle edge and the point at which the greatest transverse diameter of the
128   shell intersects the surface of the valves." Yonge (1955:404), acknowledging correspondence
129   with Owen, described the demarcation line as: "the projection onto the sagittal plane of the line
130   of maximum inflation of each valve … starting at the umbones. … i.e. the region where the ratio
131   of the transverse to radial component in the growth of the mantle/shell is greatest." Carter et al.
132   (2012:52) provided perhaps the clearest description as the line defining the "dorsoventral profile
133   when the shell is viewed from the anterior or posterior end." However, Stasek (1963*b*)
134   demonstrated the difficulty in measuring this line; note the nearly orthogonal orientations of the
135   empirically determined demarcation line on *Ensis* (Stasek 1963*b*:225-Fig.5a) compared to its
136   initially proposed position (Owen 1952:148-Fig. 5). Stasek's empirical approach, coupled with
137   the revised definition of Carter et al., is tractable with today's 3D-morphology toolkit. But,
138   critically, this definition depends on the direction of the anteroposterior axis, which itself is
139   variably defined (see discussion in next section). Thus, definitionally driven shifts in the
140   direction of the anteroposterior axis can alter the trace of the demarcation line. Owen's initial
141   definition is independent of the anteroposterior axis, but as Stasek demonstrated, its

142   identification can be unreliable. Thus, high degrees of digitization error for the demarcation line

143   may confound comparisons of shell shape, and we do not include the demarcation line as a

144   feature for aligning shells across the Class.

145   Both the directive plane and the demarcation line attempt to orient the shell on aspects of

146   its geometry that are intrinsic to its growth. A similar and more reliably determined approach

147   may be orientation to the **maximum growth axis** (i.e. **line of greatest marginal increment**

148   sensu Owen 1952; Figure 1). The maximum growth axis is the straight line that connects the

149   origin and terminus of the trace of maximum growth across the shell surface. This trace connects

150   the beak to the ventral margin along a perpendicular path to the most widely spaced

151   commarginal growth increments (as such, this definition appears to have similar properties to the

152   trace of the directive plane on the shell surface). But, as for the directive plane and the

153   demarcation line, the maximum growth axis can be prone to measurement error without fitting a

154   formal model of shell growth (e.g. those of Savazzi 1987; Ubukata 2003), and should therefore

155   be used with caution. However, a reasonable and reliably measured proxy for this axis is the line

156   lying on the commissural plane that originates at the beak and terminates at the furthest point on

157   the shell commissure. Thus, this axis can indicate the dorsoventral orientation of the shell.

158   Orientation using the **shape of the shell commissure** offers, arguably, the most reliably

159   determined approach that uses intrinsic properties of the shell (Figure 2a). Given the accretionary

160   growth of the shell, points on the commissure—the homologous leading edge of shell growth

161   (Vermeij 2013)—are geometrically homologous, or correspondent (Bookstein 1991; Gunz et al.

162   2005). Valve handedness is still required to ensure that compared valves are from the same side

163   of the body (i.e. left vs. right), which requires anteroposterior directionality (see below). This

164   alignment thus orients shells using geometric correspondence based on homology of growth.

165   The sagittal axis is crucial to the shell's three-dimensional alignment and is likely the

166   least controversially defined. This axis is the pole (=normal) to the sagittal plane, which lies

167   parallel to the commissural plane defined as: "the more proximal part of the line or area of

168   contact of the two shell valves" (Carter et al. 2012:38). Therefore, the sagittal axis is parallel to

169   the frontal and horizontal planes (Figure 1). The proximal direction is towards the commissural

170   plane and the distal direction is towards the shell's summit: the point on the shell that is

171   maximally distant from the commissural plane (Figure 1, Cox et al. 1969:108; Carter et al.

172   2012:177). If valve handedness (i.e. left vs. right laterality) and the directionality of the

173   dorsoventral and anteroposterior axes are known, then this axis is rarely required for orientation.

174   However, certain definitions of the anteroposterior and dorsoventral axes are not constrained to

175   be orthogonal (e.g. in monomyarian taxa with the anteroposterior axis defined as the oro-anal

176   axis, see below, and the dorsal ventral axis as the axis of maximum growth—*Pecten* in Figure 1);

177   as the axes representing the anteroposterior and dorsoventral directions become more parallel,

178 then the sagittal axis becomes an increasingly important safeguard against the inversion of the
179 proximal-distal direction in quantitative alignments.

2.1.2 Orientation via the soft-body as reflected on the shell

181 Anteroposterior directionality is the third Cartesian axis required for orienting the bivalve shell
182 in three-dimensions. The positions of the mouth (anterior) and anus (posterior) ultimately
183 determine the anteroposterior axis (Jackson 1890, 'preferably' described as the 'oro-anal' axis in
184 Cox et al. 1969:79), but the exact positions of these two soft-body features are rarely recorded
185 directly on the shell. Thus, tactics for determining the polarity, if not the precise bearing, of the
186 anteroposterior axis have relied on lineage or body-plan specific proxies—shell features that are
187 assumed to correlate with positions of the soft-body anatomy (e.g. positions of the adductor
188 muscle scars, Figure 1a, Cox et al. 1969:79). Disparate body plans necessitate taxon-specific
189 rules for orientation, such that determining the anterior and posterior ends of the shell requires a
190 mosaic approach. For example, there are at least three definitions of the anteroposterior axis in
191 dimyarians alone (Bailey 2009:493), which necessarily differ from those of monomyarians
192 considering the reliance on two, instead of one, adductor muscle scars. For those monomyarians,
193 which commonly have lost the anterior adductor (Yonge 1954; but see loss of the posterior
194 adductor in the protobranch Nucinellidae, Allen and Sanders 1969; Glover and Taylor 2013),
195 additional shell features are used to orient the anteroposterior axis. In pectinids, the byssal notch
196 of the anterior auricle proxies the location of the mouth (Figure 1b), but in ostreids, the mouth is
197 more centrally located under the umbo, near the beak (Yonge 1954:448).

198   Lineage or body-plan specific definitions help with anteroposterior orientation of shells
199 that lack point-based homology (e.g. two muscle scars vs. one), but they still rely on proxies for
200 the position of soft-body features that may not be determined for taxa known only from their
201 shells, e.g. some fossils (Bailey 2009). Hypothesizing anteroposterior orientation using
202 phylogenetic proximity to extant clades may help, but this approach should be used with caution
203 in given the lack of direct anatomical evidence—especially when phylogenetic affinities are
204 either unknown or distant, as for many Paleozoic taxa (Bailey 2009). Nor is it advisable to
205 assume the precise bearing of the anteroposterior axis is identical to another, well-defined axis
206 such as the hinge line (see variable bearings of the anteroposterior axis and hinge *axis* in Cox et
207 al. 1969:80-Fig. 64). However, if the phylogenetic or temporal scope of an analysis precludes the
208 determination of the anteroposterior axis using homologous body features with geometric
209 correspondences (e.g. inclusion of dimyarian and monomyarian taxa), then the hinge line offers a
210 universal proxy; that way, multiple features can be used to determine the anterior and posterior
211 ends of the shell (Cox et al. 1969).

2.2   Alignment of shells for geometric morphometrics

Our challenge here is to reconcile the many means of orienting bivalve shells discussed above into alignment schema for geometric morphometrics. We compare the differences in shell shape produced by the five orientations listed below. All five orientations use the sagittal axis (SX) to determine the lateral orientation of the shell. Precise definitions of landmark placement for each axis are provided in the Methods.

- **SX-HL-oHL.** Anteroposterior orientation determined by the hinge line (HL); dorsoventral orientation determined by the orthogonal line to the HL within the commissural plane (oHL). This alignment emulates the orientation scheme for measuring shell height, length, and width—the most common and widely applicable framework for comparing shell morphology (Cox et al. 1969:81–82; Kosnik et al. 2006).
- **SX-OAX-oOAX.** Anteroposterior orientation determined by the proxied positions of the mouth and anus using shell features (oro-anal axis, OAX); dorsoventral orientation determined by the orthogonal line to the OAX within the commissural plane (oOAX). Similar to SX-HL-oHL, this alignment largely determines orientation by a single axis, the OAX, which has also been used to frame linear measurements of shell morphology (e.g. Stanley 1970:19).
- **SX-HL-GX.** Anteroposterior orientation determined by the hinge line (HL); dorsoventral orientation determined by the maximum growth axis (GX). This alignment allows an aspect of shell growth to affect its orientation and thus the degrees of morphological similarity among specimens.
- **SX-HL-GX-OAX.** Anteroposterior orientation determined by the directions of both the HL and OAX; dorsoventral orientation determined by GX. This 'full' alignment scheme allows axes derived from intrinsic characteristics of the shell and the body to affect orientation.
- **SX-COMM.** Anteroposterior and dorsoventral orientation determined by the shape of the commissure curve, with the initial point nearest the beak (Figure 2a). This alignment uses the geometric correspondence of semilandmarks on the commissure that capture the relationship between its shape and growth.

Procrustes superimposition (or Procrustes Analysis) is the workhorse of geometric morphometrics—aligning shapes by translation to a common origin, scaling to common size, and rotation to minimize relative distances of landmarks (see variants thereof in Zelditch et al. 2012). While we are most concerned with assessing the effects of rotation using the five alignments described immediately above, choices of translation and scaling can also influence shape differences. Thus, we consider all combinations of parameter values for each step in the Procrustes Analysis. As there is arguably no objective criterion to determine which alignment

248   best suits bivalve shells, we discuss the benefits and drawbacks of each approach and

249   quantitatively compare the similarities of resulting alignments. Ultimately, we use this exercise

250   to propose a best practice for aligning bivalve shells and comparing their shapes—a process that

251   may be of use for workers in other, similarly disparate morphological systems that lack high

252   degrees of point-based homology.

253   **3.   Methods**

254   **3.1   Dataset**

255   We adopt the style of previous approaches to studying bivalve orientation and use a dataset of

256   morphological end-members to illustrate the effects of different alignment schemes (e.g. Owen

257   1952; Yonge 1954; Stasek 1963*a*). Eleven species that represent most major body plans were

258   selected to proxy the morphological and anatomical disparity across the evolutionary history of

259   the Class (Table S1). Bivalves with highly reduced shells or those that form part of a larger

260   structure (tubes and crypts) are not directly analyzed here, but we consider their fit to the

261   alignments in the Discussion.

262   One valve from an adult individual of each species was sampled from museum

263   collections (see Acknowledgments). Nine of eleven individuals are equivalve, and because we do

264   not examine details of dentition, their left and right valves are operationally mirror images of

265   each other. The inequivalve taxa included here (*Pecten*, *Ostrea*) primarily differ in terms of

266   inflation (height above the commissural plane); for the purposes of our analysis, the location of

267   key features such as the hinge area and adductor muscle scars are similar enough that using

268   either valve gives a similar orientation. Valves were scanned using micro-CT at the University of

269   Chicago's Paleo-CT facility, and three-dimensional, isosurface, triangular-mesh models were

270   created in VG Studio Max and cleaned in Rvcg (Schlager 2017) and Meshmixer. Landmarks

271   were placed using 'Pick Points' in Meshlab (Visual Computing Lab ISTI – CNR 2019). Meshes,

272   landmarks, and code necessary to reproduce the analyses here are provided in the Supplemental

273   Material.

274   **3.2   Aligning bivalve shells in a geometric morphometrics framework**

275   **3.2.1   Scaling**

276   Procrustes Analysis scales objects to a common size, and three alternative scalings are

277   considered here: (1) the **centroid size of the shell** (Figure 2b), (2) the **centroid size of the**

278   **commissure** (Figure 2a), and (3) the **volume of the shell**. The centroid size of the shell reflects

279   the 3D footprint of the shell, and the centroid size of the commissure reflects the size of the

280   shell's growth front. ==Shell volume—the amount of calcium carbonate—may be less correlated==

281 ==with shell shape than the other two measures,==and may therefore reveal shape differences not
282 intrinsically linked to size.

3.2.2 Translation

284 After scaling, Procrustes Analysis translates objects to a common origin. Objects are typically
285 'centered' by subtracting the centroid of the landmark set (mean X, Y, and Z coordinate values
286 per object) from each landmark coordinate, thus shifting the center of each landmark set to the
287 origin (X=0, Y=0, Z=0). Three points are considered for translation here: (1) the **beak** (Figure 1),
288 (2) the **centroid of the shell** (Figure 2b), and (3) the **centroid of the commissure** (Figure 2a).
289 Translation to the beak positions shells onto the homologous point of initial shell growth.
290 Translation to the centroids of the shell or its commissure incorporate more information on the
291 shape of the shell, with centering on the commissure adding an aspect of homology by
292 positioning shells on their growth front. Operationally, Procrustes Analysis translates landmark
293 sets to their respective centroids before minimizing their rotational distances, overriding any
294 prescribed translations; the three translations above are therefore implemented after the rotation
295 step (following the functionality in *Morpho::procSym* Schlager 2017).

3.2.3 Rotation

297 Rotation in Procrustes Analysis orients landmark coordinates to minimize their pairwise sum of
298 squared distances. The 5 orientations discussed in the introduction were used for rotation.
299 Because Procrustes Analysis uses Cartesian coordinates, two landmarks were placed on the mesh
300 surface of a shell to indicate the direction of each axis as described in the subsections below
301 (exact placement of landmarks on specimens in Figure S1).

Sagittal orientation

303 *Sagittal axis [SX].* This axis is the pole to the commissural plane (Figure 1). It is determined as
304 the average cross product of successive vectors that originate at the centroid of the commissure
305 and terminate at semilandmarks on the commissure curve (visualization of fitting the
306 commissural plane in Figure S2). The distal direction is towards the exterior surface of the shell
307 and the proximal direction is towards the interior surface.

Anteroposterior orientation

309 *Hinge line [HL].* The hinge line is determined by landmarks placed at the two farthest apart
310 articulating elements of the hinge area (Figure 1). The landmarks are then designated as being
311 anterior or posterior using the available discriminating features on the shell and can thus proxy
312 the anteroposterior orientation. While not an 'axis' in the strict anatomical sense, we group the
313 hinge line with the other anatomical axes below.

314 *Oro-anal axis [OAX].* The positions of the mouth and anus or proxies thereof are used to orient
315 the oro-anal axis and thus the anteroposterior orientation. For dimyarian taxa, anterior and
316 posterior ends of the axis are determined by landmarks placed on the dorsal-most edge of the
317 anterior and posterior adductor muscle scars (Figure 1a, the 'Type 2 adductor axis' of Bailey
318 2009:493 after Stanley 1970:19). For monomyarian taxa that have retained the posterior adductor
319 muscle, the centroid of that adductor muscle scar is landmarked as the posterior end of the axis
320 and shell features that reflect the position of the mouth are landmarked as the anterior end (e.g.
321 the ventral notch of the anterior auricle in pectinids [Figure 1b] or the beak in ostreids, Yonge
322 1954). The axis is reversed in monomyarian taxa that have retained the anterior muscle (e.g. the
323 protobranch Nucinellidae, Glover and Taylor 2013).

324 **Dorsoventral orientation**

325 *Maximum growth axis [GX].* The origin of shell growth at the beak is the dorsal landmark on the
326 maximum growth axis and the point on the shell commissure with the greatest linear distance to
327 the beak is ventral landmark (Figure 1).

328 *Orthogonal hinge line [oHL].* By definition, the orthogonal line to the HL (oHL) represents the
329 dorsoventral axis, with the dorsal-most point nearest the beak.

330 *Orthogonal oro-anal axis [oAX].* By definition, the orthogonal axis to the OAX (oOAX)
331 represents the dorsoventral axis, with the dorsal-most point nearest the beak.

332 **Commissure orientation**

333 The manually placed landmarks on the shell commissure were used to fit a three-dimensional
334 spline on which 50 equally spaced semilandmarks were placed in an anterior direction
335 (clockwise for left valves when viewed towards the interior surface, counterclockwise for right
336 valves). The semilandmark on the commissure curve nearest the beak landmark was selected as
337 the initial point (Figure 2a). Semilandmarks were then slid to minimize bending energy and
338 reduce artifactual differences in shape driven by their initial, equidistant placement (Gunz et al.
339 2005; Gunz and Mitteroecker 2013; Schlager 2017).

340 **Standardized axis points**

341 We observed that variance among specimens in the distances between the axis landmarks
342 notably influenced their best-fit orientation in the Procrustes Analysis (see difference in spacing
343 of these landmarks in Figure S1). To remove this 'Pinocchio effect' (*sensu* Zelditch et al.
344 2012:67), axis landmarks were 'standardized' (visualization of this process in Figure 3). The
345 vector defined by the two axis landmarks was shifted to the centroid of the shell commissure and
346 normalized to unit length; the standardized axis points (we explicitly avoid calling them
347 landmarks) were then designated by the terminal points of the unit vector and its negative.

348 Standardized axis points result in alignments that better reflect the collective impacts of axis
349 direction, not magnitude.

3.3 Alignment and comparison of shape differences

351 Meshes and landmark sets for right valves were mirrored across their commissural plane and
352 analyzed as operational left valves. This is a reasonable approach for equivalve taxa when
353 analyzing general shell shape, e.g. of the interior or exterior surfaces, but homologous valves
354 should be used for analyses that include inequivalve taxa as, by definition, their two shapes
355 differ. Landmark sets were then scaled, rotated, and translated (in that order) under all possible
356 parameter combinations outlined in the preceding section, totaling 45 alignment schemes.
357 Landmark coordinate values were scaled by dividing the landmark coordinates by a specimen's
358 size (e.g. centroid size or volume). Scaled landmarks were then temporarily centered on the
359 centroid of the commissure and then rotated via the respective orientation scheme using
360 Generalized Procrustes Analysis (*Morpho:procSym*, Schlager 2017); scaling during this step was
361 explicitly disallowed. Lastly, scaled and rotated landmarks were translated to one of the three
362 target locations (i.e. the beak or centroids of the commissure semilandmarks or shell points).

363 Similarity of alignments was quantified using the metric distances between the shapes of
364 interior shell surfaces, which were used to reduce the impact of exterior ornamentation on the
365 differences in general shell shape. Sliding semilandmarks on the commissure and the interior
366 surface of the shell were used to capture 'shape.' Initially, for the commissure, 50 equidistant
367 semilandmarks were placed and the curve's starting point was determined by the orientation
368 scheme (e.g. starting at the semilandmark nearest the beak for the SX-COMM orientation, see
369 details in Supplemental Text §2.3, Figure S5); for the interior surface, semilandmarks were
370 placed at proportionate distances along the dorsoventral and anteroposterior axes of each
371 orientation scheme (5% distance used here, which results in 420 semilandmarks; see details and
372 step-by-step visualization in Supplemental Text §2.3, Figure S3, Figure S4, Figure S5). Mixing
373 the orientations of semilandmarks and rotation axes may be useful for comparing the interaction
374 of growth and anatomical direction with shell shape, but this approach can result in unintuitive,
375 and perhaps unintended, shape differences among specimens. After placement of equidistant
376 semilandmarks, those on the commissure curve were slid to minimize their thin-plate spline
377 bending energy and then used to bound the sliding of the surface semilandmarks (Figure S5;
378 Gunz et al. 2005; Gunz and Mitteroecker 2013; implemented via *Morpho::slider3d*, Schlager
379 2017). The final sliding semilandmark set consisted of 430 landmarks (50 points on the
380 commissure plus the 380 points on the surface grid which do not lie on the commissure, i.e. the
381 non-edge points; Figure S5). Landmark coverage analyses may be used at this point to maximize
382 downstream statistical power (Watanabe 2018), but we relied on qualitative assessment of shape
383 complexity and landmark coverage for the simple analyses conducted here.

384   For each of the 45 alignments, ==similarity in shell shape was calculated as the pairwise==
385   ==Euclidean distances of the sliding surface semilandmarks==. Identical shapes have a distance of
386   zero. Pairwise distances between shapes for each alignment scheme were normalized by their
387   respective standard deviations, making the distances between specimens comparable across
388   alignments. These normalized pairwise distances were then compared in three ways. First, a
389   permutation-based multivariate analysis of variance (==perMANOVA as implemented by==
390   *==geomorph::procD.lm==*, Adams et al. 2021) was used to model the effects of Procrustes Analysis
391   steps on the scaled pairwise distances between specimens. Each of the 45 rows in the analyzed
392   matrix was a unique Procrustes Analysis treatment, or alignment—i.e. a combination of scaling,
393   rotation, and translation—and each of the 55 columns was a scaled distance between a pair of the
394   eleven specimens. Second, this alignment matrix was scaled and centered and Principal
395   Components Analysis was conducted to visualize the individual and joint effects treatments
396   across alignments (i.e. Figure 4). Third, 'hive diagrams' (see network plots in Figure 5d) were
397   used to compare the scaled pairwise distances of specimens among selected alignments to a
398   reference alignment, where scaling = centroid of commissure, rotation = HL-oHL, translation =
399   centroid of shell commissure.

400   **4.   Results and Discussion**

401   All three Procrustes Analysis steps—translation, scaling, and rotation—significantly affect the
402   alignments of shells (~~Table1~~, visualized as clustering of steps in Figure 4). As defined in the
403   Methods, quantitative similarity in alignment was determined using the scaled, pairwise
404   Euclidean distances among the sliding semilandmarks placed on the interior surface of the shell.
405   Treatments within steps (e.g. translation to the beak vs. centroid of the shell) differentiate
406   alignments while the effects of other parameters are held constant ($p=0.001$ for all parameters,
407   Table1). Scaling most strongly differentiates alignments, with rotation and translation having
408   smaller effects (see standardized effect sizes as Z scores in Table1). It follows that the
409   differences between alignments are smallest among rotation and translation treatments (i.e. the
410   smallest distances between alignments reflected as the lowest Sum of Squares, Table1, see also
411   their clustering in Figure 4), and they increase for treatments of scaling. These metric differences
412   among alignments are informative for understanding the impacts of individual steps in Procrustes
413   Analysis, but visually comparing the orientations of shells is necessary to understand an
414   alignment's fidelity to biological homology and/or analogy.

415   **4.1   Effects of translation**

416   The choice of translation can change how differences in shell shape are interpreted. Translation
417   to the beak, the lone homologous point across the class, allows the comparison of shell shapes
418   conditioned on directions of growth from their origins (Figure 5c). *Ensis* can be described as
419   being posteriorly elongated compared to *Glycymeris*, or *Pecten* as 'taller' than *Pholas* from the

420 beak to the ventral margin. Still, translation to the beak can exaggerate or bias the differences in
421 'pure' shell shape. For example, *Ensis* and *Tagelus* have greater distances between their shapes
422 when translated to the beak than to the centroid of commissure semilandmarks (red line in
423 Figure 5d.iii). Their offset positions of the beak underlies this difference, which is interesting for
424 analyses of growth vs. shape, but the shape of the shell, irrespective of its growth, is arguably the
425 primary target of ecological selection (Stanley 1970, 1975, 1988; Vermeij 2002; Seilacher and
426 Gishlick 2014). Thus, measuring the morphological similarity of shells for studies of
427 ecomorphology, trends in disparity, or evolutionary convergence would be best conducted using
428 translation to their respective centroids of the commissure or shell surface (Figure 5a,b); these
429 two translations yield very similar alignments given the close proximity of their respective
430 centroids (as shown by the pale colors linking specimens in Figure 5d.ii; but note the small offset
431 between the two centroids for the more irregularly shaped *Cuspidaria*). In general, it is best
432 practice to translate shells to their respective centroids of the commissure semilandmarks or shell
433 points when morphological analyses target differences in pure shell shape. Translation to the
434 centroid of the commissure is preferred because it incorporates homology into the alignment via
435 correspondence of the leading edge of shell growth.

4.2   Effects of scaling

437 Scaling has a large effect on the differences between alignments (see largest Sum of Squares for
438 the term in the ANOVA, Table1). Scaling by volume leaves particularly large residual
439 differences in shape; the most voluminous shells are made extremely minute (*Pecten* and
440 *Tridacna* in particular, Figure 6c) while the least voluminous shells become the largest
441 (*Nuculana* and *Cuspidaria*). Scaling to logged shell volume does not alleviate these residual
442 differences (results not shown), and, moreover, the aim of this scaling step is to remove the
443 isometric relationship of size to shape, not its allometric one. The relative sizes of specimens are
444 more similar when scaled to the centroid size of the commissure semilandmarks or the shell
445 points (Figure 6a,b). These two sizes are tightly correlated (Figure S6) and thus produce very
446 similar alignments (Figure 6d.ii). For comparing differences in overall shell morphology in 3D,
447 scaling by the centroid size of shell points would best equalize the isometric differences in size
448 among specimens, thus concentrating the remaining differences in morphology to their shapes.

4.3   Effects of rotation

450 Of the three Procrustes Analysis parameters, rotation is arguably the most important factor
451 defining the biological basis for differences in shell shape. Visually, rotation treatments can
452 produce nearly orthogonal orientations of specimens (compare the nearly orthogonal orientation
453 of the traditional shell length axis for *Ensis* and *Tagelus* between SX-HL-oHL and SX-COMM,
454 Figure 7a,e; also reflected in the deep-red bar linking these two taxa in Figure 7f.v and is spacing
455 of specimens on the first two PC axes in Figure S7). Equilateral shells are aligned similarly

456 across rotation treatments (compare orientations of *Glycymeris*, *Pecten,* and *Tridacna*, cf. *Ostrea*,
457 in Figure 7a-e and the less saturated lines connecting them in Figure 7e.ii-v). Differences in
458 alignments become more pronounced among the more inequilateral shells (seen to a minor extent
459 in *Chione* relative to *Glycymeris* and *Pecten*, but notably in *Modiolus, Pholas, Cuspidaria,* and
460 *Ensis*). Thus, alignments of inequilateral shells tend to reflect a compromise between the often
461 subparallel but not orthogonal orientations of their axes (most clearly seen in the changes to the
462 orientation of *Modiolus*, *Pholas*, and *Ensis* relative to *Glycymeris* and *Pecten* in Figure 7a-f).
463 Rotation by sliding semilandmarks on the commissure results in a similar alignment of most
464 shells to the hinge line orientation (pale lines in Figure 7e.v), but the relative shape differences of
465 *Modiolus*, *Ensis*, and *Tagelus* indicate the importance and impact of the beak position. The
466 commissure curve begins at the point nearest the beak, which affects the orientation of the
467 surface semilandmark grid (see Figure S5). Thus, in the SX-COMM treatment, the growth and
468 therefore 'shape' of *Modiolus* and *Ensis* is more similar to the tall-shelled *Ostrea* than either are
469 to the putative, similarly elongate *Pholas* and *Tagelus* (which themselves become more
470 dissimilar in shape owing to the slight offset in their beak positions). Overall, rotation using the
471 hinge axis and its orthogonal axis as the pseudo dorsoventral axis is likely the best practice for
472 most analyses of shell shape, as discussed below.

4.4 Practical alignments for bivalve shells

474   The axis-based approach to alignment (Figure 7a-d) is useful both for its ability to
475 encompass broad phylogenetic analyses of shell morphology and for its ability to combine extant
476 and fossil data, the latter known almost exclusively from shells. All shell morphologies should fit
477 within this scheme, including those with strong lateral asymmetry (e.g. rudists, see Jablonski
478 2020, and those with calcified tubes or crypts (teredinids and clavagellids, Morton 1985; Savazzi
479 1999, each of which have identifiable valves with anatomical axes—whether to include the tubes
480 and crypts as aspects of shell morphology is a different debate). With increasing phylogenetic
481 proximity, the number of point-based biological homologies is likely to increase, permitting
482 more traditional approaches to specimen alignment (Roopnarine 1995; Roopnarine et al. 2008;
483 Márquez et al. 2010; Serb et al. 2011; Collins et al. 2013, 2020; Edie et al. 2022; Milla Carmona
484 et al. First View). These shell-based axes and features (Figure 7a-e) are also useful for
485 incorporating fossil taxa into analyses with extant taxa (Yonge 1954; Cox et al. 1969; Stanley
486 1970; Bailey 2009), but aspects of the internal anatomy remain crucial for orientation (Stasek
487 1963*a*), especially the designation of the anterior and posterior ends. Fortunately, in many cases
488 the anteroposterior axis can be determined from imprints of the soft anatomy on the shell surface
489 (e.g. the pallial sinus) or from other shell features (e.g. siphonal canals, pedal gapes). This
490 necessarily variable and often idiosyncratic approach to defining the direction of anatomical axes
491 may result in more digitization error than seen in traditional point-based geometric
492 morphometrics. However, the impact of that error on analytical interpretations of shape

493　similarity and variance will depend on the overall scale of shape disparity; for analyses of
494　morphology across the class, the latter is likely to far exceed the former.

495　　　In biological systems with limited homology in a strict, point-based, geometric sense—
496　and even in those with plenty of it—numerous approaches have been used to align specimens for
497　morphological analysis. A single solution likely does not exist, and comparisons among different
498　methods will be the most powerful approach to testing evolutionary hypotheses (see Bromham
499　2016 for the necessity of comparative analyses in historical science). As for most analytical
500　frameworks, comparisons of shell shape will require explicit definition of the alignment scheme
501　and interpretation of any differences within those boundaries. Thus, we cannot declare outright
502　that one of these alignment schemes is logically superior, but we do recognize a practical
503　solution that, to us, best reflects the decades of study of shell morphology: alignment via the
504　sagittal axis, hinge line, and its orthogonal line as the pseudo dorsoventral axis (SX-HL-oHL).
505　Shell height, length, and width have been the principal measurements for analyzing differences
506　in shape, and long-standing, taxon-specific 'rules' have become entrenched in the literature and
507　therefore influence our interpretations of the clade's evolutionary morphology (see discussion in
508　Cox et al. 1969:81–82 and the continued utility of these measurements in Kosnik et al. 2006).
509　The SX-HL-oHL rotation tends to orient shells according to the defined axes of those linear
510　measurements. Of course, precedent need not dictate the course of future work, but here, we find
511　it reasonable to align this 'next generation' of shell shape analyses with the long-standing
512　conventions in the literature, if only for comparative purposes.

513　**5.　Conclusions**

514　The debate on how to align specimens is still relevant in the current era of morphometry, where
515　comparisons of animal form are increasingly accessible in 2D, 3D, and even 4D (Boyer et al.
516　2016; Olsen et al. 2017; Pearson et al. 2020). But, no matter how shapes are compared,
517　interpretations of their differences or variances should be with respect to an assumed anatomical
518　alignment. For comparisons of disparate morphologies, particularly those that lack biological
519　homology conducive to point-based landmarking, alignments will likely require non-standard
520　approaches so that shape differences do not depend on geometric correspondence alone. In
521　bivalves, anatomical axes inferred from taxon-specific features offer a class-wide approach to
522　orientation. One set of axes in particular (HL-SX-DVX) coincides with historical approaches to
523　their morphometry, while another offers new insight into the relationship between shell shape
524　and shell growth (COMM-SX). Either of these solutions are valid in their own way. This
525　philosophy of specimen alignment may be particularly relevant to other model systems in
526　paleobiology and macroevolution that have accretionary-style growth: gastropods, brachiopods,
527　corals, bryozoans, etc.—each with limited point-based landmarks corresponding to biological
528　homology.

529 **6. Acknowledgments**

535 **8. Data Availability**

536 Mesh models, landmark data, and code for reproducing analyses and figures available from
537 Zenodo: 10.5281/zenodo.6326531; mesh models also available from Morphosource Project ID:
538 000429826 (ARK IDs of specimens in Table S1).

539 **9. Authors' contributions**

540 SME and KSC designed the study, SME performed analyses, all authors contributed to the
541 writing.

542 **10. References**

543 Adams, D. C., M. L. Collyer, A. Kaliontzopoulou, and E. K. Baken. 2021: Geomorph: Software
544 for geometric morphometric analyses. R package version 4.0. https://cran.r-
545 project.org/web/packages/geomorph/index.html

546 Allen, J. A., and H. L. Sanders. 1969: *Nucinella serrei* Lamy (Bivalvia: Protobranchia), A
547 monomyarian solemyid and possible living actinodont. Malacologia 7:381–396.

548 Bailey, J. B. 2009: Shell orientation terminology among the Bivalvia (Mollusca): Problems and
549 proposed solutions. Journal of Paleontology 83:493–495.

550 Bardua, C., R. N. Felice, A. Watanabe, A.-C. Fabre, and A. Goswami. 2019: A practical guide to
551 sliding and surface semilandmarks in morphometric analyses. Integrative Organismal
552 Biology 1:obz016.

553 Bookstein, F. L. 1991: Landmarks. Pp. 55–87 *in* Morphometric Tools for Landmark Data:
554 Geometry and Biology. Cambridge University Press, Cambridge.

555 Borras, A., J. Pascual, and J. C. Senar. 2000: What do different bill measures measure and what
556 is the best method to use in granivorous birds? Journal of Field Ornithology 71:606–611.

557 Boyer, D. M., G. F. Gunnell, S. Kaufman, and T. M. McGeary. 2016: Morphosource: Archiving
558 and sharing 3-D digital specimen data. The Paleontological Society Papers 22:157–181.

559 Bradshaw, J. D., and M. A. Bradshaw. 1971: Functional morphology of some fossil
560 palaeotaxodont bivalve hinges as a guide to orientation. Palaeontology 14:242–249.

561 Bromham, L. 2016: Testing hypotheses in macroevolution. Studies in History and Philosophy of

562   Science Part A 55:47–59.

563   Carter, J. G., P. J. Harries, N. Malchus, A. F. Sartori, L. C. Anderson, R. Bieler, A. E. Bogan, E.
564   V. Coan, J. C. W. Cope, S. M. Cragg, J. R. García-March, J. Hylleberg, P. Kelley, K.
565   Kleemann, C. McRoberts, P. M. Mikkelsen, J. Pojeta, W. Skelton, I. Tëmkin, T. Yancey,
566   and A. Zieritz. 2012: Illustrated glossary of the Bivalvia. Treatise Online No. 48, Part N,
567   Revised, Volume 1, Chapter 31:1–209.

568   Carter, R. M. 1967: On the nature and definition of the lunule, escutcheon and corcelet in the
569   Bivalvia. Journal of Molluscan Studies 37:243–263.

570   Collins, K. S., J. S. Crampton, and M. Hannah. 2013: Identification and independence:
571   Morphometrics of Cenozoic New Zealand *Spissatella* and *Eucrassatella* (Bivalvia,
572   Crassatellidae). Paleobiology 39:525–537.

573   Collins, K. S., S. M. Edie, and D. Jablonski. 2020: Hinge and ecomorphology of *Legumen*
574   Conrad, 1858 (Bivalvia, Veneridae), and the contraction of venerid morphospace
575   following the end-Cretaceous extinction. Journal of Paleontology 94:489–497.

576   Cox, L. R., C. P. Nuttall, and E. R. Trueman. 1969: General features of Bivalvia. Pp. 2–129 *in* R.
577   C. Moore, ed. Treatise of Invertebrate Paleontology. Part N, Mollusca 6, Bivalvia. Vol. 1.
578   Geological Society of America & University of Kansas, Boulder, CO & Lawrence, KS.

579   Crame, J. A. 2020: Early Cenozoic evolution of the latitudinal diversity gradient. Earth-Science
580   Reviews 202:103090.

581   Edie, S. M., D. Jablonski, and J. W. Valentine. 2018: Contrasting responses of functional
582   diversity to major losses in taxonomic diversity. Proceedings of the National Academy of
583   Sciences U.S.A. 115:732–737.

584   Edie, S. M., S. C. Khouja, K. S. Collins, N. M. A. Crouch, and D. Jablonski. 2022: Evolutionary
585   modularity, integration and disparity in an accretionary skeleton: Analysis of venerid
586   Bivalvia. Proceedings of the Royal Society B: Biological Sciences 289:20211199.

587   Fang, Z., and T. M. Sanchez. 2012: Origin and early evolution of the Bivalvia. Treatise Online
588   no. 43: Part N, Revised, Volume 1, Chapter 16:1–21.

589   Glover, E. A., and J. D. Taylor. 2013: A new shallow water species of *Nucinella* from the
590   Philippines (Bivalvia: Protobranchia: Nucinellidae), member of a tropical seagrass
591   chemosynthetic community. The Nautilus 127:101–106.

592   Gunz, P., and P. Mitteroecker. 2013: Semilandmarks: A method for quantifying curves and
593   surfaces. Hystrix, the Italian Journal of Mammalogy 24:103–109.

594   Gunz, P., P. Mitteroecker, and F. L. Bookstein. 2005: Semilandmarks in three dimensions. Pp.
595   73–98 *in* D. E. Slice, ed. Modern Morphometrics in Physical Anthropology. Kluwer
596   Academic Publishers-Plenum Publishers, New York.

597   Jablonski, D. 2020: Developmental bias, macroevolution, and the fossil record. Evolution &
598   Development 22:103–125.

599 Jablonski, D., S. Huang, K. Roy, and J. W. Valentine. 2017: Shaping the latitudinal diversity
600   gradient: New perspectives from a synthesis of paleobiology and biogeography.
601   American Naturalist 189:1–12.
602 Jackson, R. T. 1890: Phylogeny of the Pelecypoda: The Aviculidae and their allies. Memoirs of
603   the Boston Society of Natural History 4:277–400.
604 Kosnik, M. A., D. Jablonski, R. Lockwood, and P. M. Novack-Gottshall. 2006: Quantifying
605   molluscan body size in evolutionary and ecological analyses: Maximizing the return on
606   data-collection efforts. PALAIOS 21:588–597.
607 Lison, L. 1949: Recherches sur la forme et la mécanique de développement des coquilles des
608   Lamellibranches. Mémoires Institut royal des Sciences Naturelles de Belgique 34:3–87.
609 Marin, F., N. Le Roy, and B. Marie. 2012: The formation and mineralization of mollusk shell.
610   Frontiers in Bioscience (Schol. Ed.) S4:1099–1125.
611 Márquez, F., R. Amoroso, M. Gowland Sainz, and S. Van der Molen. 2010: Shell morphology
612   changes in the scallop *Aequipecten tehuelchus* during its life span: A geometric
613   morphometric approach. Aquatic Biology 11:149–155.
614 Mikkelsen, P. M., R. Bieler, I. Kappner, and T. A. Rawlings. 2006: Phylogeny of Veneroidea
615   (Mollusca: Bivalvia) based on morphology and molecules. Zoological Journal of the
616   Linnean Society 148:439–521.
617 Milla Carmona, P. S., D. G. Lazo, and I. M. Soto. First View: Ontogeny in the steinmanellines
618   (Bivalvia: Trigoniida): An intra- and interspecific appraisal using the Early Cretaceous
619   faunas from the Neuquén Basin as a case study. Paleobiology.
620 Morton, B. 1985: Adaptive radiation in the Anomalodesmata. Pp. 405–459 *in* The Mollusca,
621   Vol. 10, Evolution. Elsevier.
622 Morton, J. E., and C. M. Yonge. 1964: Classification and structure of the Mollusca. Pp. 1–58 *in*
623   K. M. Wilbur and C. M. Yonge, eds. Physiology of Mollusca. Vol. 1. Elsevier, New
624   York.
625 Olsen, A. M., A. L. Camp, and E. L. Brainerd. 2017: The opercular mouth-opening mechanism
626   of largemouth bass functions as a 3D four-bar linkage with three degrees of freedom.
627   Journal of Experimental Biology 220:4612–4623.
628 Owen, G. 1952: Shell-form in the Lamellibranchia. Nature 170:148–149.
629 Pearson, K. D., G. Nelson, M. F. J. Aronson, P. Bonnet, L. Brenskelle, C. C. Davis, E. G. Denny,
630   E. R. Ellwood, H. Goëau, J. M. Heberling, A. Joly, T. Lorieul, S. J. Mazer, E. K.
631   Meineke, B. J. Stucky, P. Sweeney, A. E. White, and P. S. Soltis. 2020: Machine learning
632   using digitized herbarium specimens to advance phenological research. BioScience
633   70:610–620.
634 Roopnarine, P. D. 1995: A re-evaluation of evolutionary stasis between the bivalve species
635   *Chione erosa* and *Chione cancellata* (Bivalvia: Veneridae). Journal of Paleontology

636 69:280–287.

637 Roopnarine, P. D., J. Signorelli, and C. Laumer. 2008: Systematic, biogeographic, and
638   microhabitat-based morphometric variation of the bivalve *Anomalocardia squamosa*
639   (Bivalvia: Veneridae: Chioninae) in Thailand. The Raffles Bulletin of Zoology 18:90–98.

640 Savazzi, E. 1987: Geometric and functional constraints on bivalve shell morphology. Lethaia
641   20:293–306.

642 Savazzi, E. 1999: Borng, nestling and tube-dwelling bivalves. Pp. 205–237 *in* Functional
643   Morphology of the Invertebrate Skeleton. John Wiley & Sons, Chichester.

644 Scarlato, O. A., and Y. I. Starobogatov. 1978: Phylogenetic relations and the early evolution of
645   the Class Bivalvia. Philosophical Transactions of the Royal Society B: Biological
646   Sciences 284:217–224.

647 Schlager, S. 2017: Morpho and Rvcg – Shape analysis in R: R-Packages for geometric
648   morphometrics, shape analysis and surface manipulations. Pp. 217–256 *in* G. Zheng, S.
649   Li, and G. Székely, eds. Statistical Shape and Deformation Analysis: Methods,
650   Implementation and Applications. Academic Press, London, UK.

651 Seilacher, A., and A. D. Gishlick. 2014: Morphodynamics. CRC Press, Boca Raton, FL.

652 Serb, J. M., A. Alejandrino, E. Otárola-Castillo, and D. C. Adams. 2011: Morphological
653   convergence of shell shape in distantly related scallop species (Mollusca: Pectinidae).
654   Zoological Journal of the Linnean Society 163:571–584.

655 Stanley, S. M. 1970: Relation of shell form to life habits of the Bivalvia (Mollusca). Geological
656   Society of America Memoirs 125:1–282.

657 ———. 1975: Why clams have the shape they have: An experimental analysis of burrowing.
658   Paleobiology 1:48–58.

659 ———. 1988: Adaptive morphology of the shell in bivalves and gastropods. Pp. 105–141 *in* E.
660   R. Trueman and M. R. Clarke, eds. The Mollusca Vol. 11, Form and Function. Academic
661   Press, San Diego.

662 Stasek, C. R. 1963a: Orientation and form in the bivalved Mollusca. Journal of Morphology
663   112:195–214.

664 Stasek, C. R. 1963b: Geometrical form and gnomonic growth in the bivalved Mollusca. Journal
665   of Morphology 112:215–231.

666 Taylor, J. D., and E. Glover. 2021: Biology, Evolution and Generic Review of the
667   Chemosymbiotic Bivalve Family Lucinidae. Series 182, The Ray Society, London, UK.

668 Trueman, E. R. 1964: Adaptive morphology in palaeoecological interpretation. Pp. 45–74 *in* J.
669   Imbrie and N. D. Newell, eds. Approaches to Paleontology. Wiley, New York.

670 Ubukata, T. 2003: Pattern of growth rate around aperture and shell form in Bivalvia: A
671   theoretical morphological study. Paleobiology 29:480–491.

672 Vermeij, G. J. 2002: Characters in context: Molluscan shells and the forces that mold them.

673   Paleobiology 28:41–54.

674 Vermeij, G. J. 2013: Molluscan marginalia: Hidden morphological diversity at the bivalve shell
675   edge. Journal of Molluscan Studies 79:283–295.

676 Visual Computing Lab ISTI – CNR. 2019: Meshlab. https://www.meshlab.net

677 Waller, T. R. 1998: Origin of the molluscan class Bivalvia and a phylogeny of major groups. Pp.
678   1–45 *in* P. Johnston and J. Haggart, eds. Bivalves: An Eon of Evolution. Vol. 1.
679   University of Calgary Press, Calgary.

680 Watanabe, A. 2018: How many landmarks are enough to characterize shape and size variation?
681   PLOS ONE 13:e0198341.

682 Yonge, C. M. 1954: The monomyarian condition in the Lamellibranchia. Transactions of the
683   Royal Society of Edinburgh 62:443–478.

684 Yonge, C. M. 1955: Adaptation to rock boring in *Botula* and *Lithophaga* (Lamellibranchia,
685   Mytilidae) with a discussion on the evolution of this habit. Quarterly Journal of
686   Microscopical Science 96:383–410.

687 Zelditch, M. L., D. L. Swiderski, and H. D. Sheets. 2012: Geometric Morphometrics for
688   Biologists: A Primer. 2nd ed. Academic Press, San Diego, CA.

689 **9.   Table and Figure Captions**

690 **Figure 1.** Positions of shell features, axes, and planes as mentioned and defined in text for: (a) a
691 helicospiral shell *Chione elevata* (Say 1822), and (b) a more planispiral shell *Pecten maximus*
692 (Linnaeus 1767).

693 **Figure 2.** (a) Representation of shell commissure curve, its centroid, and the semilandmarks used
694 in the COMM orientation scheme. Analyses use 50 sliding semilandmarks on the commissure
695 curve, but only a subset is shown here for clarity. (b) Equally spaced points on the shell surface
696 placed using a Poisson Disc sampler (*Rvcg::vcgSample*, Schlager 2017) and their centroid. The
697 number and location of vertices on triangular meshes can vary, which strongly influences the
698 calculation of centroid size. Analyses use 2000 equally spaced points to minimize this issue
699 (only a subset of those points shown here). Figured shell is *Chione elevata*.

700 **Figure 3.** Visualization of procedure used to standardize the orientation axes defined by
701 landmarks. Figured shell is *Chione elevata*.

702 **Table 1.** Permutation multivariate analysis of variance of the scaled pairwise distances between
703 specimens across the 45 Procrustes Analysis alignments.

704 **Figure 4.** Principal Components Analysis of forty-five alignments (represented by points).
705 Spacing of alignments along the first three axes that describe 84.3% of the total variance reflects
706 the results of the MANOVA in Table1. Scaling by shell volume vs. the centroid size of either the
707 shell points or the commissure separate along PC1; together, PCs 2 and 3 show the clustering of
708 alignments with SX-COMM rotation, translation to the beak, the similarity of translation to the

709   centroids of the commissure semilandmarks and shell points, and separation of the axis-based
710   rotation schemes.

711   **Figure 5.** Effects of translation on differences in shell shapes. All shells are scaled to the
712   centroid size of the shell points and rotated using the SX-HL-oHL scheme. For individual images
713   of shells, the intersection of the gray line segments marks the origin of the Cartesian coordinate
714   system and thus the operational 'center' of the shell. **(a)** Translation to the centroid of the 2000
715   equidistant points placed on the mesh surface of the shell. **(b)** Translation of shells to the
716   centroid of the 50 semilandmark curve along the shell commissure. **(c)** Translation of shells to
717   the apex of the beak landmark, the initial point of shell growth. **(d)** *(i)* The scaled pairwise
718   Euclidean distances of semilandmarks placed on the interior surface of the shell, scaled to the
719   centroid size of the shell points and translated to the centroid of the shell commissure. 'Hotter'
720   colors indicate greater relative distances between specimens. *(ii-iii)* The difference in scaled
721   distance of specimens for the specified translation from the reference treatment in panel *i*. More
722   saturated reds indicate an increase in scaled distance relative to the reference alignment;
723   conversely, more saturated blues indicate a decrease in distance; white indicates no difference.
724   For example, *Ensis* and *Tagelus* become more dissimilar in interior shell shape when translated
725   to their respective beaks than when each are translated to their centroid of the commissure.

726   **Figure 6.** Effects of scaling on differences in shell shapes. All shells are translated centroid of
727   the commissure semilandmarks and rotated using the SX-HL-oHL scheme. Compare differences
728   in scaled sizes of specimens across rows, not columns. **(a)** Shells scaled by the centroid size of
729   the 2000 equidistant points placed on the surface of the shell mesh. **(b)** Shells scaled to the
730   centroid size of the 50 semilandmark curve along the shell commissure. **(c)** Shells scaled by the
731   volume of shell carbonate. **(d)** As in Figure 5d but based on differences in scaling.

732   **Figure 7.** Effects of rotation on differences in shell shapes. All shells are translated centroid of
733   the commissure semilandmarks and scaled to the centroid size of the shell points. Highlighted
734   colors of panel titles correspond to axes plotted on shells. To facilitate relative comparisons of
735   shell shape across columns, shells in each row were rotated such that the 'x' axis is parallel to the
736   hinge line of *Glycymeris*; this is an ad-hoc, global rotation that does not change between-
737   specimen differences in shell shape. **(a)** Shells rotated by their sagittal axis, hinge line, and
738   orthogonal hinge line as the pseudo dorsoventral axis. **(b)** Shells rotated by their sagittal axis,
739   oro-anal axis, and orthogonal oro-anal axis as the pseudo dorsoventral axis. **(c)** Shells rotated by
740   their sagittal, hinge, and maximum growth axes. **(d)** Shells rotated by their sagittal, hinge,
741   maximum growth, and oro-anal axes **(e)** Shells rotated by their sagittal axis and commissure
742   semilandmarks. **(f)** As in Figure 5d but based on differences in rotation. See Figure S7 for a
743   projection of shell shape differences along the first two principal components.

Figure 1

Positions of shell features, axes, and planes as mentioned and defined in text for: (a) a helicospiral shell *Chione elevata*(Say 1822), and (b) a more planispiral shell *Pecten maximus* (Linnaeus 1767).
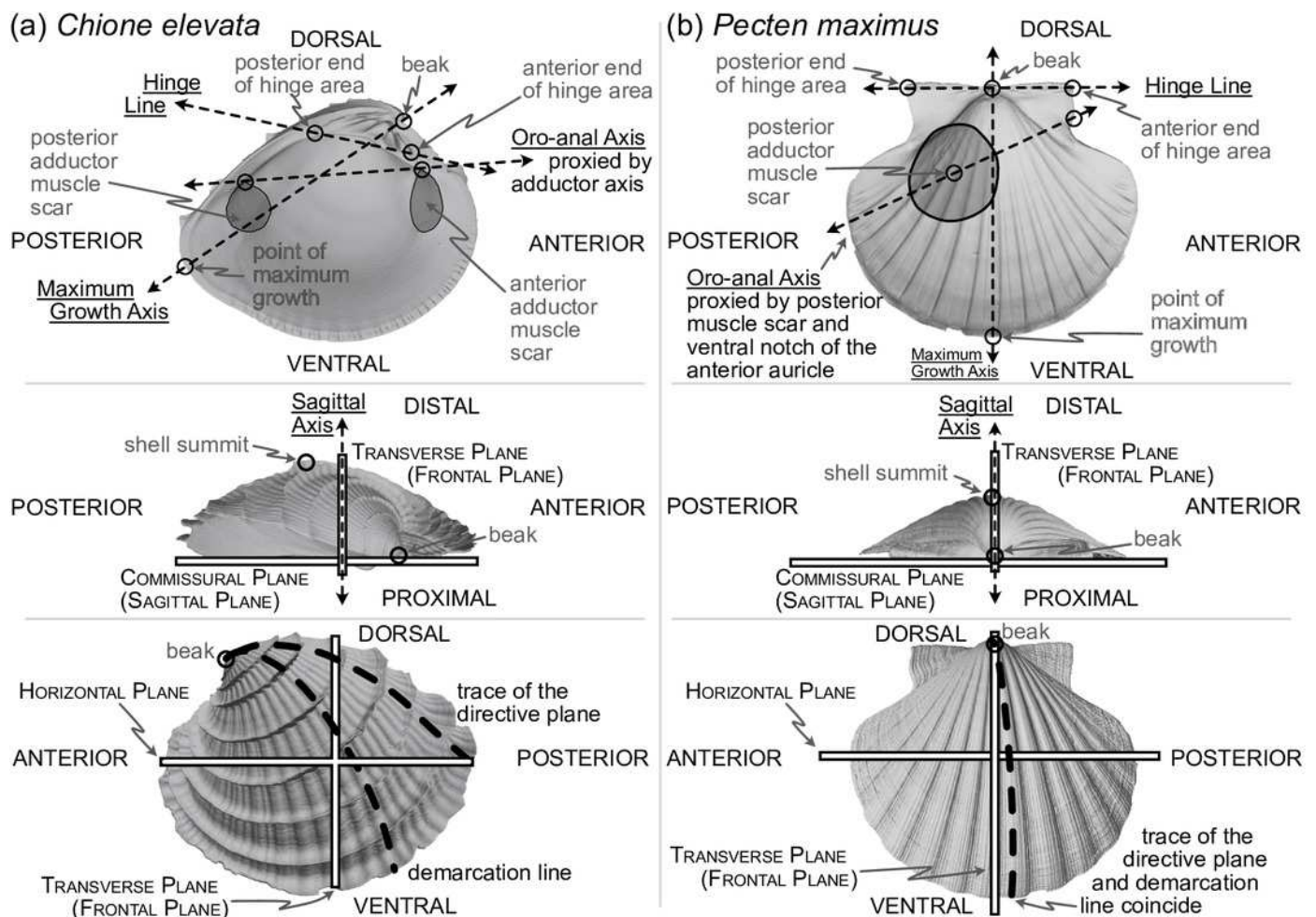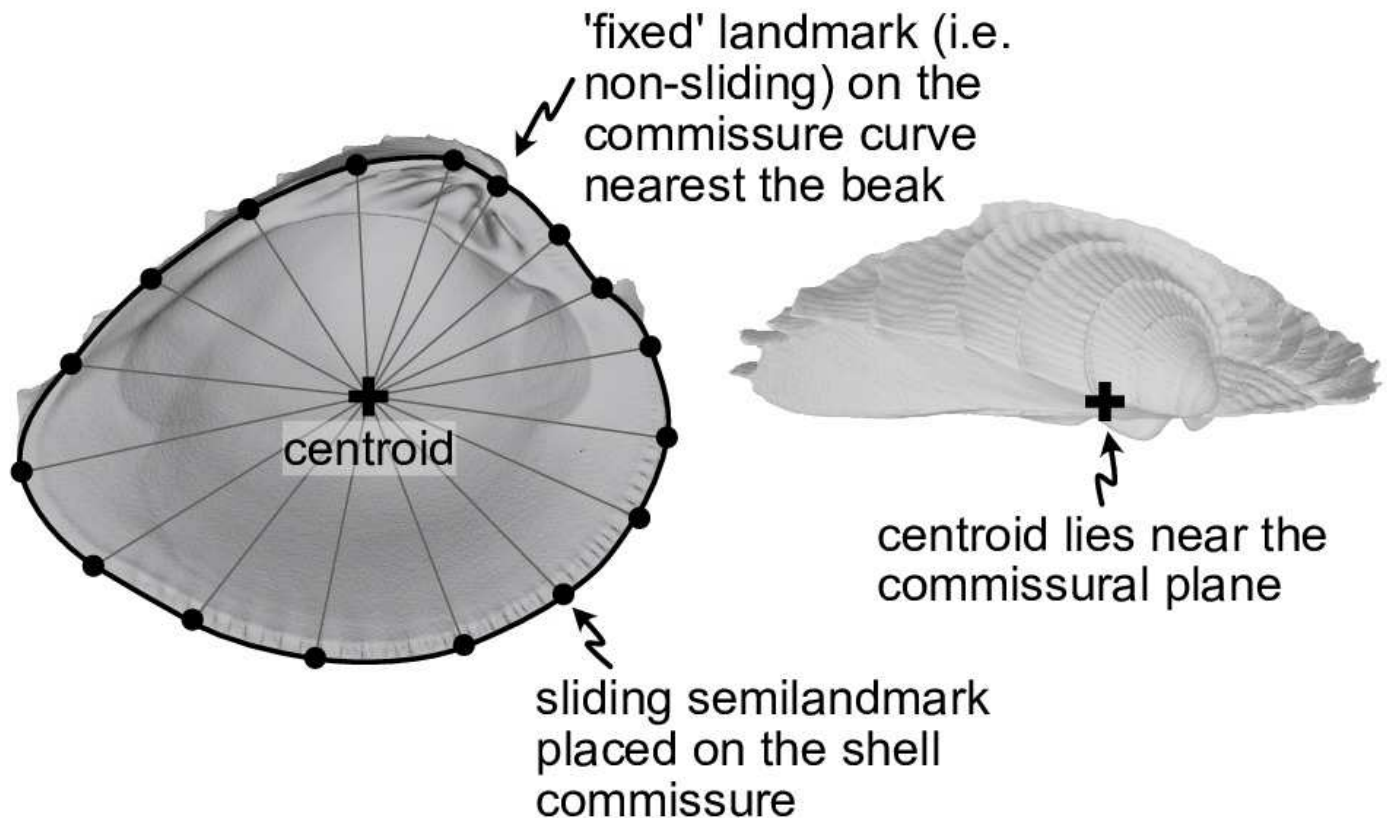
Figure 2

Definition of shell commissure and centroids.

(a) Representation of shell commissure curve, its centroid, and the semilandmarks used in the COMM orientation scheme. Analyses use 50 sliding semilandmarks on the commissure curve, but only a subset is shown here for clarity. (b) Equally spaced points on the shell surface placed using a Poisson Disc sampler (*Rvcg::vcgSample*, Schlager 2017) and their centroid. The number and location of vertices on triangular meshes can vary, which strongly influences the calculation of centroid size. Analyses use 2000 equally spaced points to minimize this issue (only a subset of those points shown here). Figured shell is *Chione elevata*.

(a) Commissure curve semilandmarks and their centroid

'fixed' landmark (i.e. non-sliding) on the commissure curve nearest the beak

centroid

centroid lies near the commissural plane

sliding semilandmark placed on the shell commissure

(b) Shell points and their centroid

evenly spaced point on shell surface used to calculate centroid

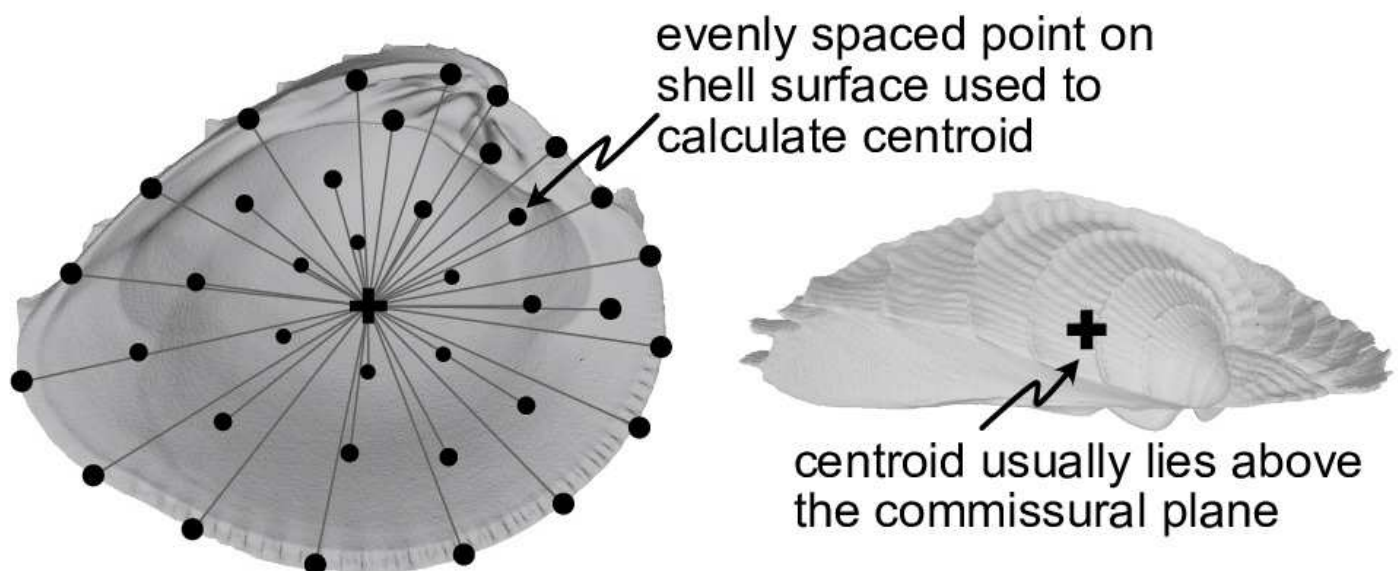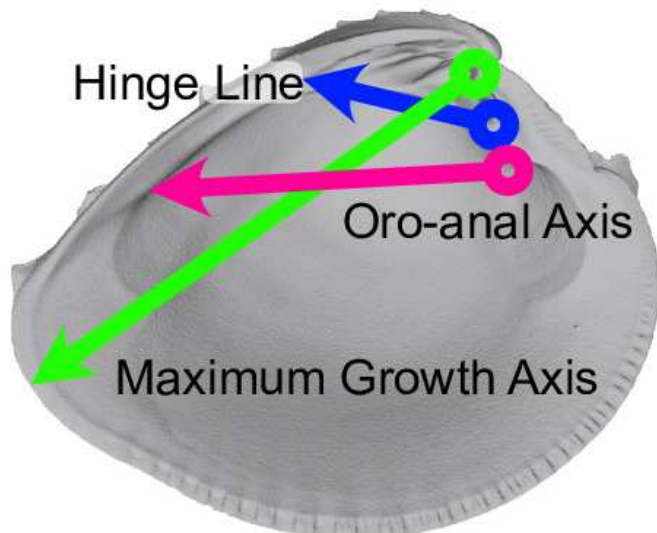centroid usually lies above the commissural plane

Figure 3

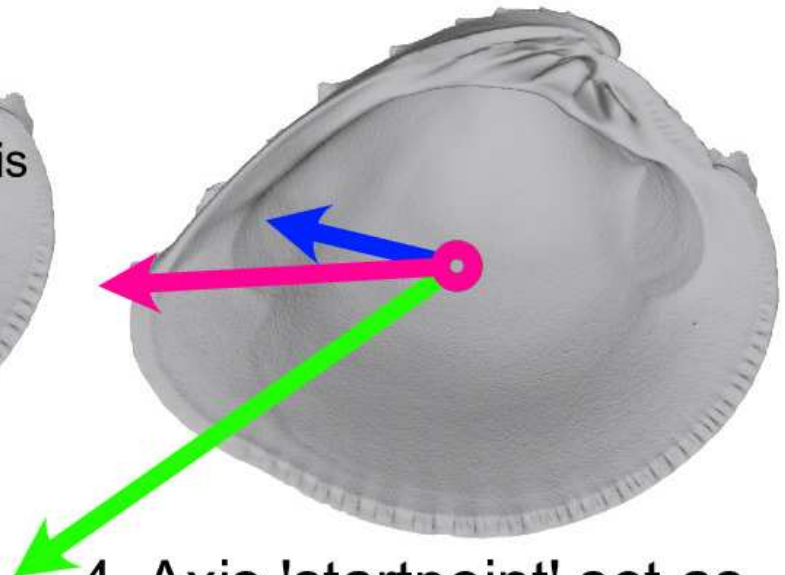Visualization of procedure used to standardize the orientation axes defined by landmarks.

Figured shell is *Chione elevata*.

Standardization of axes defined by landmarks

1. Landmarks placed to set axis orientation.

Hinge Line

Oro-anal Axis

Maximum Growth Axis

2. Initial points shifted to the centroid of the commissure.

3. Axis 'vectors' normalized to unit length, then duplicated and multiplied by -1 (dashed 'negative' vectors).
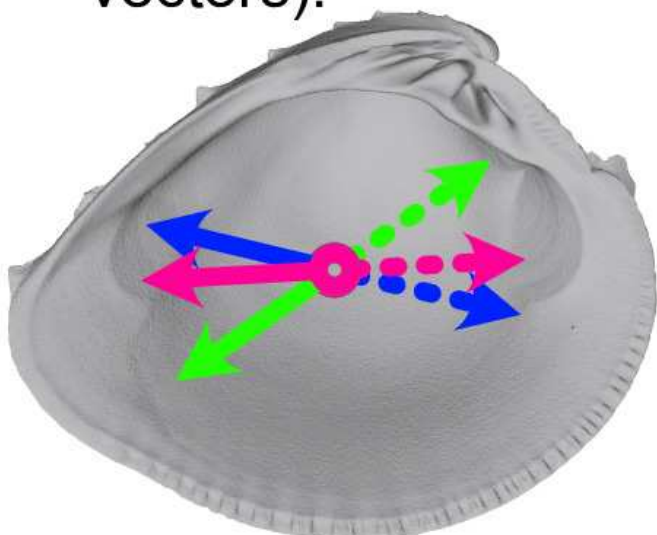
4. Axis 'startpoint' set as the terminal point of the negative vector and axis 'endpoint' set as terminal point of original vector.
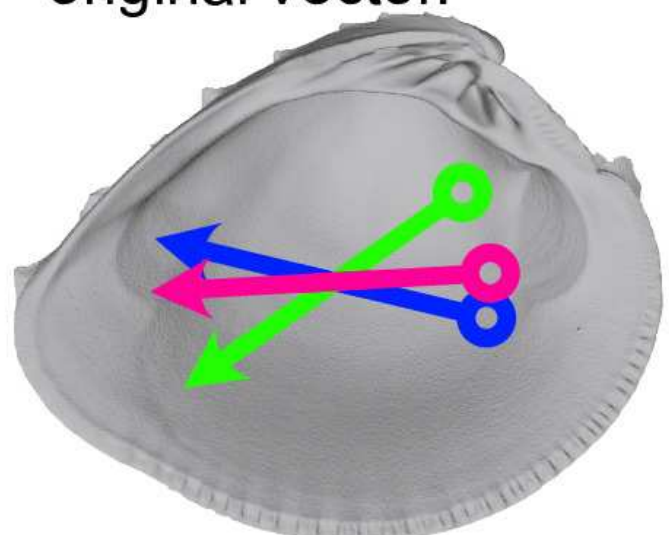
Figure 4

Principal Components Analysis of forty-five alignments (represented by points).

Spacing of alignments along the first three axes that describe 84.3% of the total variance reflects the results of the MANOVA in Table1. Scaling by shell volume vs. the centroid size of either the shell points or the commissure separate along PC1; together, PCs 2 and 3 show the clustering of alignments with SX-COMM rotation, translation to the beak, the similarity of translation to the centroids of the commissure semilandmarks and shell points, and separation of the axis-based rotation schemes.

Figure 5

Effects of translation on differences in shell shapes.

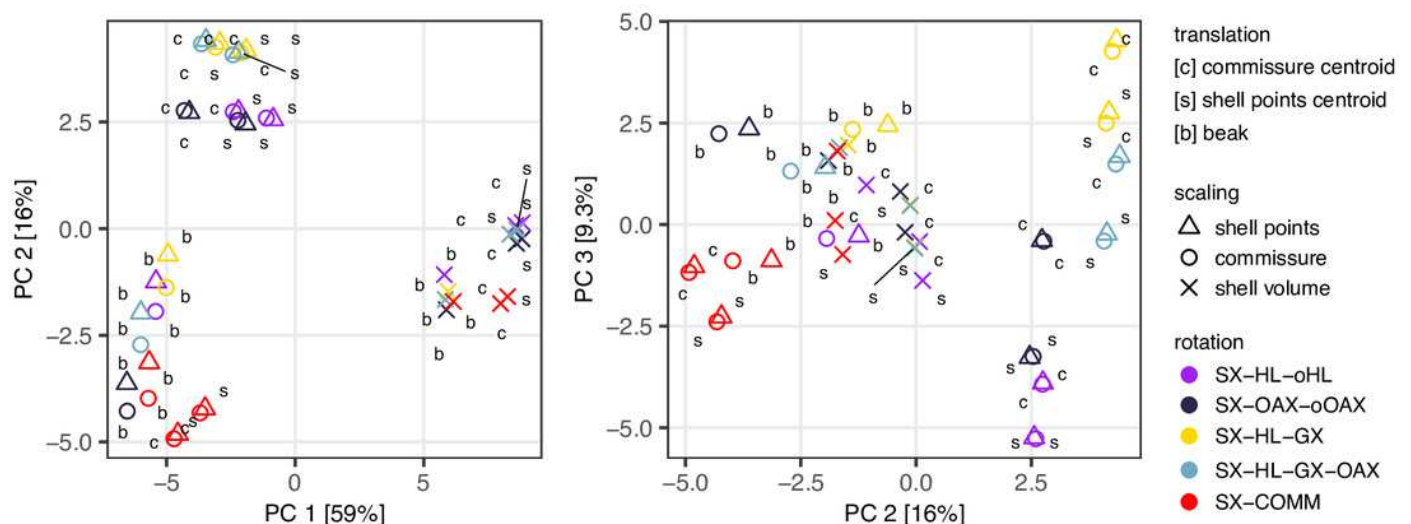All shells are scaled to the centroid size of the shell points and rotated using the SX-HL-oHL scheme. For individual images of shells, the intersection of the gray line segments marks the origin of the Cartesian coordinate system and thus the operational 'center' of the shell. **(a)** Translation to the centroid of the 2000 equidistant points placed on the mesh surface of the shell. **(b)** Translation of shells to the centroid of the 50 semilandmark curve along the shell commissure. **(c)**Translation of shells to the apex of the beak landmark, the initial point of shell growth. **(d)** *(i)* The scaled pairwise Euclidean distances of semilandmarks placed on the interior surface of the shell, scaled to the centroid size of the shell points and translated to the centroid of the shell commissure. 'Hotter' colors indicate greater relative distances between specimens. *(ii-iii)* The difference in scaled distance of specimens for the specified translation from the reference treatment in panel *i*. More saturated reds indicate an increase in scaled distance relative to the reference alignment; conversely, more saturated blues indicate a decrease in distance; white indicates no difference. For example, *Ensis* and *Tagelus* become more dissimilar in interior shell shape when translated to their respective beaks than when each are translated to their centroid of the commissure.

(a) Translation to centroid of shell commissure points

Glycymeris Pecten Tridacna Chione Ostrea Modiolus Nuculana Pholas Cuspidaria Ensis Tagelus

(b) Translation to centroid of shell points

(c) Translation to beak landmark

(d) Metric distances between specimens

(i) Reference translation: Centroid of shell commissure points

(ii) Translation to centroid of shell points

(iii) Translation to beak

scaled Euclidean distance between specimens
more similar shapes ← → less similar shapes
0.5 1.0 1.5

difference in scaled distance from reference alignment
shapes less different than in reference alignment ← → shapes more different than in reference alignment
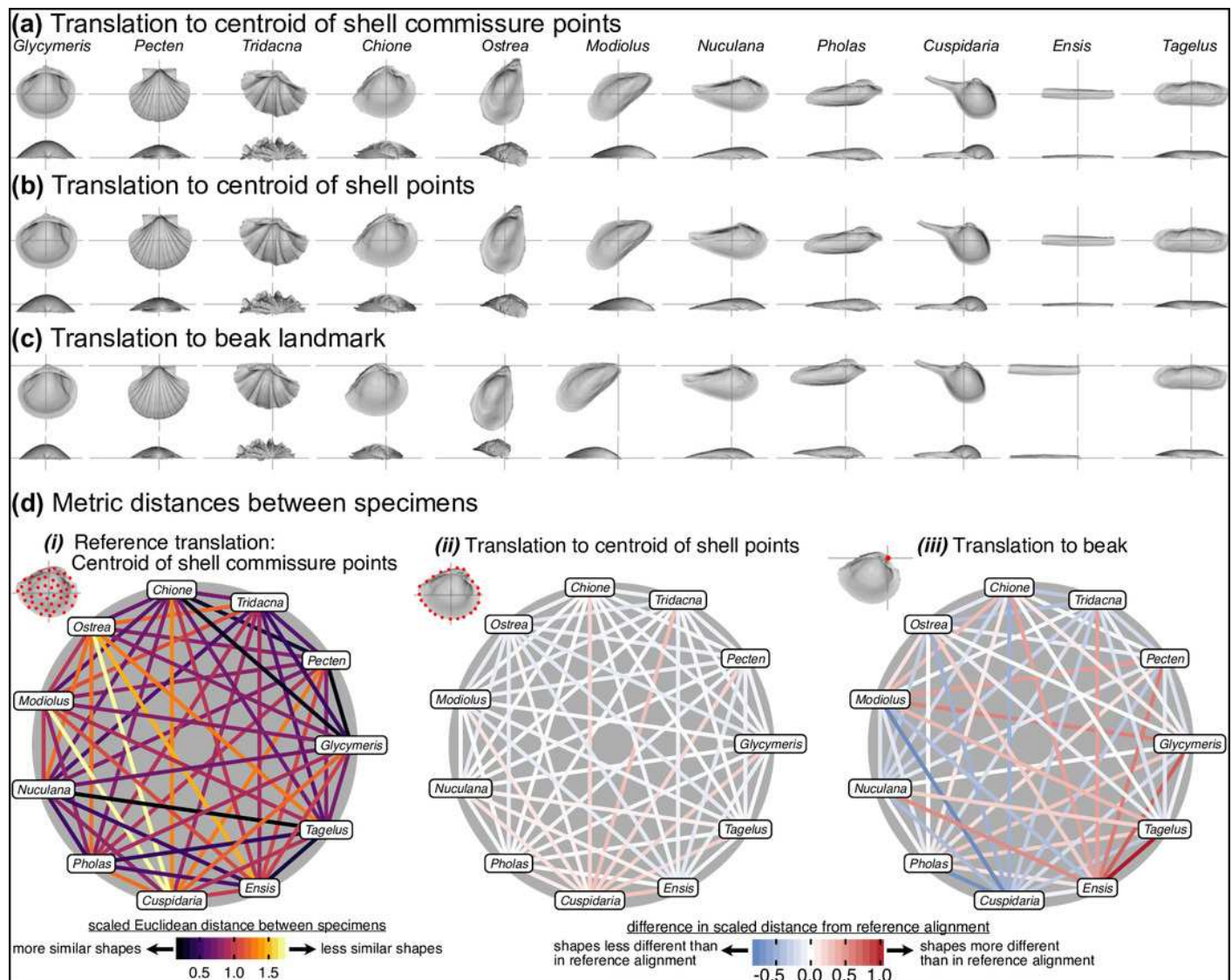-0.5 0.0 0.5 1.0

Figure 6

Effects of scaling on differences in shell shapes.

All shells are translated centroid of the commissure semilandmarks and rotated using the SX-HL-oHL scheme. Compare differences in scaled sizes of specimens across rows, not columns. **(a)** Shells scaled by the centroid size of the 2000 equidistant points placed on the surface of the shell mesh. **(b)** Shells scaled to the centroid size of the 50 semilandmark curve along the shell commissure. **(c)** Shells scaled by the volume of shell carbonate. **(d)** As in Figure 5d but based on differences in scaling.
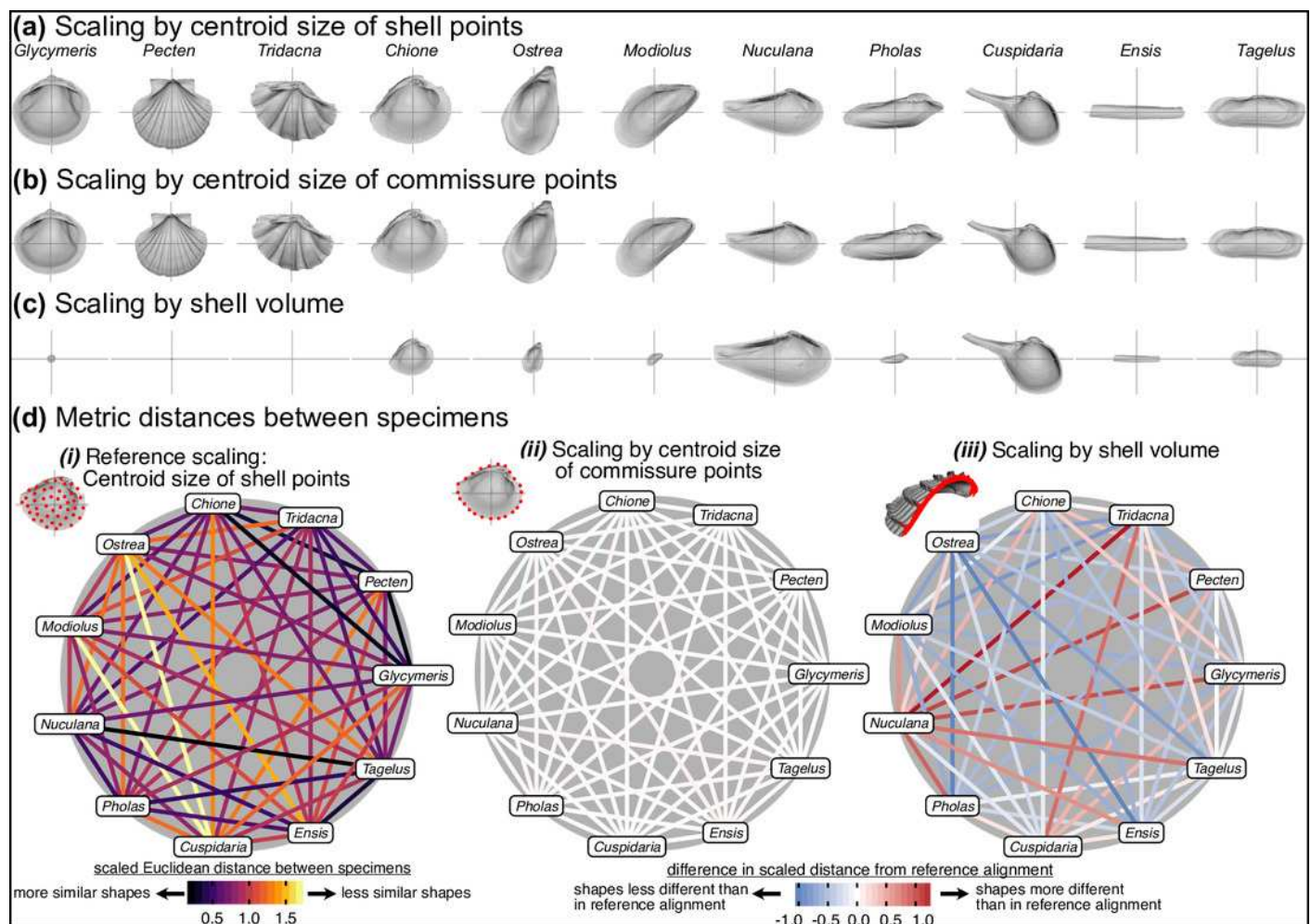
Figure 7

Effects of rotation on differences in shell shapes.

All shells are translated centroid of the commissure semilandmarks and scaled to the centroid size of the shell points. Highlighted colors of panel titles correspond to axes plotted on shells. To facilitate relative comparisons of shell shape across columns, shells in each row were rotated such that the 'x' axis is parallel to the hinge line of *Glycymeris*; this is an ad-hoc, global rotation that does not change between-specimen differences in shell shape. **(a)** Shells rotated by their sagittal axis, hinge line, and orthogonal hinge line as the pseudo dorsoventral axis. **(b)** Shells rotated by their sagittal axis, oro-anal axis, and orthogonal oro-anal axis as the pseudo dorsoventral axis. **(c)** Shells rotated by their sagittal, hinge, and maximum growth axes. **(d)** Shells rotated by their sagittal, hinge, maximum growth, and oro-anal axes **(e)** Shells rotated by their sagittal axis and commissure semilandmarks. **(f)** As in Figure 5d but based on differences in rotation. See Figure S7 for a projection of shell shape differences along the first two principal components.

(a) [SX-HX-oHX] Alignment by sagittal axis (SX: pole to visible plane), hinge line (HL), orthogonal hinge line (oHL)

(b) [SX-OAX-oOAX] Alignment by SX, oro-anal axis (OAX), orthogonal oro-anal axis (oOAX)

(c) [SX-HL-GX] Alignment by SX, HL, maximum growth axis (GX)

(d) [SX-HL-GX-OAX] Alignment by SX, HL, GX, OAX

(e) [SX-COMM] Alignment by SX, commissure sliding semilandmarks (COMM)

(f) Metric distances between specimens

(i) Reference rotation: SX-HL-oHL
(ii) Rotated via SX-OAX-oOAX
(iii) Rotated via SX-HL-GX
(iv) Rotated via SX-HL-GX-OAX
(v) Rotated via SX-COMM

scaled Euclidean distance between specimens
more similar shapes ← → less similar shapes
0.5 1.0 1.5

difference in scaled distance from reference alignment
shapes less different than in reference alignment ← → shapes more different than in reference alignment
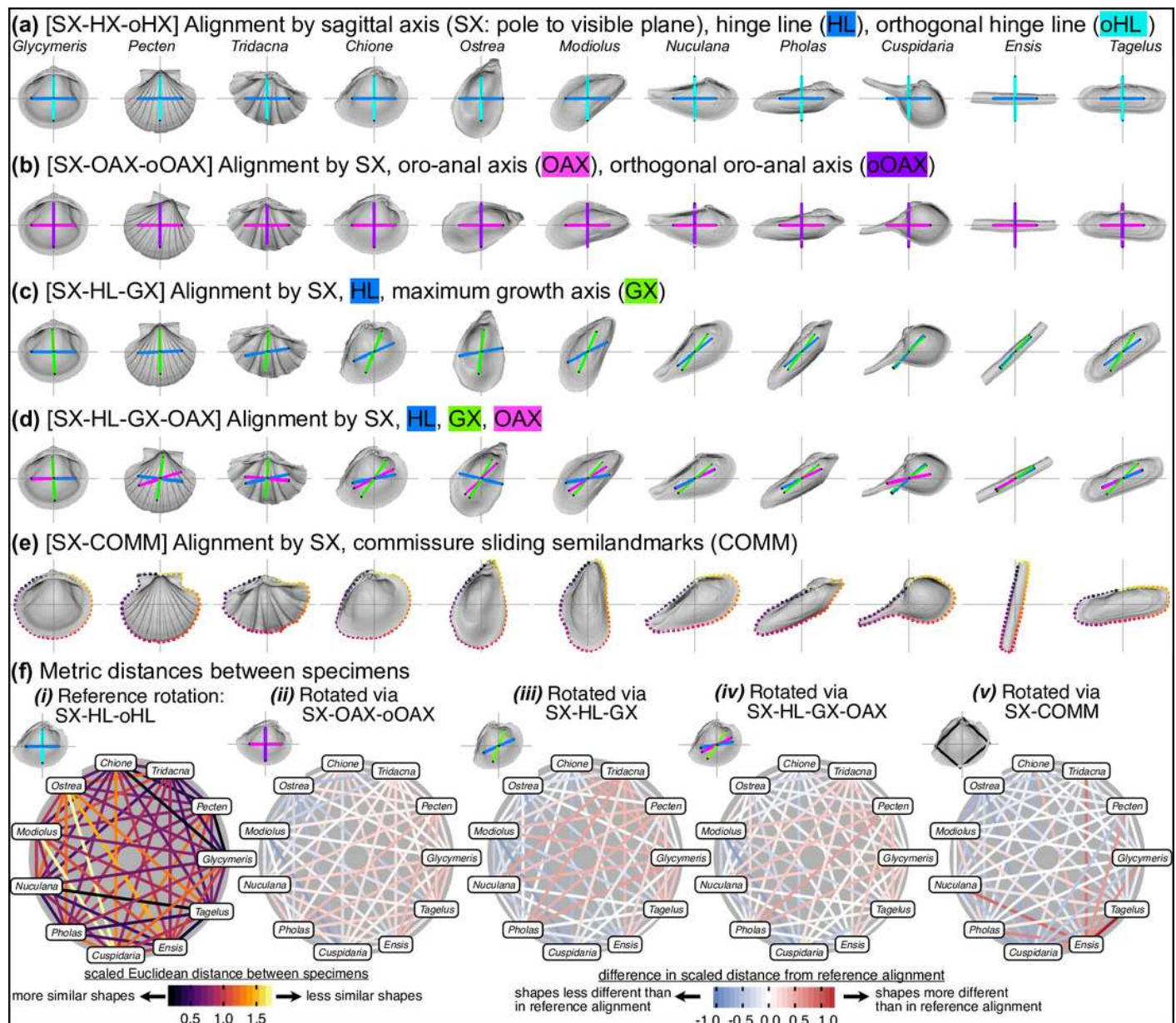-1.0 -0.5 0.0 0.5 1.0

Table 1(on next page)

Permutation multivariate analysis of variance of the scaled pairwise distances between specimens across the 45 Procrustes Analysis alignments.

Term	df	Sum of Squares	Mean Square	R²	F	Z	p
translation	2	30.6	15.3	0.11	13.7	4.4	0.001
scaling	2	185.4	92.7	0.64	82.7	6.2	0.001
rotation	4	34.7	8.7	0.12	7.7	4.8	0.001
Residuals	36	40.3	1.1	0.14			
Total	44	291					

1